Revision 2

Stability of fcc phase FeH to 137 GPa

CHIE KATO[1,2,*] , KOICHIRO UMEMOTO[2], KENJI OHTA[1], SHOH TAGAWA[3],
KEI HIROSE[2,3], and YASUO OHISHI[4]

[1]Department of Earth and Planetary Sciences, Tokyo Institute of Technology, 2-12-1
Ookayama, Meguro, Tokyo, 152-8550, Japan

[2]Earth-Life Science Institute, Tokyo Institute of Technology, 2-12-1 Ookayama, Meguro,
Tokyo, 152-8550, Japan

[3]Department of Earth and Planetary Science, The University of Tokyo, 7-3-1 Hongo,
Bunkyo, Tokyo, 113-0033, Japan

[4]Japan Synchrotron Radiation Research Institute, 1-1-1 Koto, Sayo, Hyogo, 679-5198,
Japan

*E-mail: chiekato15@gmail.com

ABSTRACT

We examined the stable crystal structure of FeH_X (X~1) (FeH hereafter) at high pressure and temperature by X-ray diffraction up to 137 GPa. Results show that FeH adopts a face-centered cubic (fcc) structure at pressures of 43 to 137 GPa and temperatures of approximately 1000 to 2000 K. Our study revises a phase diagram of stoichiometric FeH in which fcc has a wider-than-expected stability field at high pressure and temperature. Based on our findings, the FeH endmember of the Fe-FeH system is expected to be stable in the fcc structure at the *P-T* conditions of the Earth's core, rather than in the double-hexagonal close packed (dhcp) structure as previously reported. We compared experimentally determined FeH lattice volumes with those from *ab initio* calculations. Additionally, we observed a change in compressibility at ~60 GPa, which could be attributed to a magnetic transition - an interpretation supported by our *ab initio* computations.

Keywords: FeH, fcc structure, Earth's core, X-ray diffraction, *ab initio* calculation

INTRODUCTION

Hydrogen is a possible constituent light element within the Earth's predominantly iron-nickel core (e.g., Poirier, 1994). Therefore, evaluation of the Fe–FeH system under the high pressure (*P*) and high temperature (*T*) conditions of the Earth's deep interior is important in the discussion of chemical and physical properties of the core. An endmember of this system, stoichiometric FeH with double-hexagonal close packed (dhcp) structure, has been observed in iron loaded in a hydrogen pressure medium at pressures exceeding 3.5 GPa at room temperature (e.g., Badding et al. 1991). The temperature-induced phase transition from dhcp to face centered cubic (fcc) was observed up to 20 GPa in a multi-anvil apparatus (Ikuta et al. 2019; Saitoh et al. 2017; Sakamaki et al. 2009). Locations of the melting curve and the dhcp/fcc phase boundary predict the triple point of dhcp, fcc, and liquid phases FeH at about 60 GPa and 2000 K, and the disappearance of the fcc stability field at higher pressures. Room-temperature compression experiments observed no structural change in dhcp FeH up to 136 GPa, but they did not involve thermal annealing during compression, and so lack concrete evidence for the stability of dhcp at such a pressure range (Badding et al. 1991; Hirao et al. 2004; Pépin et al. 2014; Shibazaki et al. 2012). On the other hand, there are experimental and theoretical reports that suggest fcc FeH is stable above 80 GPa and up to 1800 K (Isaev et al. 2007; Thompson et al. 2018). Free-energy calculations suggested that, at room temperature, FeH undergoes a structural transition from dhcp to hexagonal close packed (hcp) at 37 GPa, and a second transition from hcp to fcc occurs at 83 GPa (Isaev et al. 2007). They also found that a ferromagnetic-paramagnetic transition takes place at ~60 GPa in metastable fcc FeH, which leads to the change in compressibility and stabilizes the fcc structure (Isaev et al. 2007).

In addition to endmember FeH, non-stoichiometric FeH_X ($X<1$) has been identified in both the fcc structure (Thompson et al. 2018) and the hcp structure (Antonov et al. 1998; Yuan et al. 2018; Machida et al. 2019). Additionally, Fe polyhydrides with FeH_2, FeH_3, and FeH_5 composition have been reported (Pépin et al. 2014; 2017), and FeH_4 and FeH_6 have also been suggested as potential Fe-H compounds at high pressure (Bazhanova et al. 2012; Kvashnin et al. 2018).

In this study, we performed synchrotron X-ray diffraction experiments *in-situ* at high *P-T* in a laser-heated diamond anvil cell (LHDAC) to pursue the stability field of stoichiometric fcc FeH. These experiments confirmed that fcc FeH is stable up to 137 GPa and about 1000 K. We also collected lattice volume data of fcc FeH with changing pressure and found anomalous compression behavior at around 60 GPa. Based on our *ab initio* calculations, the magnetic transition in fcc FeH reasonably explains the observed change in compressibility.

METHODS

We employed the LHDAC technique to generate high *P*-*T* conditions. Diamond anvils with 300 or 120 μm diameter culets were used, and gaskets were pre-indented rhenium plate. We used two different methods to supply hydrogen to the iron foil starting material (99.99% purity). In runs #1–3, iron hydride was formed by loading an iron foil with a paraffin (C_nH_{2n+2}, n>5) pressure medium into the LHDAC with ruby or KCl pressure markers (Narygina et al. 2011; Ohta et al. 2019; Thompson et al. 2018; Hirose et al., 2019). In runs #4–8, liquid H_2 was introduced into the LHDAC and compressed with an iron foil and a NaCl inner gasket at ~20 K in a helium refrigerator (Chi et al. 2011; Ohta et al. 2015; Tagawa et al. 2016). The NaCl inner gasket prevents hydrogen embrittlement of the Re gasket and the escape of hydrogen from a sample chamber. The surface of the diamond anvils was coated with a thin Ti film to prevent the hydrogen from escaping into the anvils. Supplemental Fig. S1 shows the sample chamber after the liquid H_2 injection.

In-situ angle-dispersive X-ray diffraction (XRD) measurements were performed at BL10XU, SPring-8. XRD patterns were collected on a flat panel detector. The wavelength of the monochromatic X-ray was determined using a CeO_2 standard. Two-dimensional XRD images were integrated over the Debye-Scherrer rings to convert one-dimensional diffraction patterns as a function of 2-theta angle, and the obtained peak profiles were fit to pseudo-Voigt peak shapes. These procedures were performed on the programs of IPAnalyzer and PDindexer (Seto et al. 2010). The lattice parameters were obtained by a least-squares fit of XRD peak positions. Sample pressure was determined from ruby fluorescence spectrum (Dorogokupets and Oganov 2007) for run #1 and from the lattice volumes of KCl (Dewaele et al. 2012) and NaCl (Ueda et al. 2008) for runs #2–3 and #4–8, respectively. Dewaele et al. (2012) used the Ruby pressure scale by Dorogokupets and Oganov (2007) to obtain their equation of state of

KCl. To correct the systematic pressure difference between the equations of state of KCl and NaCl, simultaneous lattice volume measurements of KCl and NaCl were also performed (Table S1). The simultaneous lattice volume measurements of NaCl and KCl demonstrated that the difference in pressure calculated from these two standards was 0.3 GPa at 52 GPa and 13.4 GPa at 133 GPa. We fitted such a pressure difference to the following equation; $P_{\mathrm{KCl}} - P_{\mathrm{NaCl}} = \mathrm{a} \times \exp(P_{\mathrm{KCl}} / \mathrm{b})$, and obtained a = 0.058(17) GPa and b = 26.9(15) GPa. Heating was performed from both sides of the sample by employing a pair of 100 W single-mode Yb fiber lasers. Temperatures were measured by spectroradiometric method (Ohishi et al. 2008).

The hydrogen content of $\mathrm{FeH_X}$ was estimated based on the volume expansion by hydrogen incorporation at each pressure:

$$\mathrm{X} = [V(\mathrm{fcc\ FeH_X}) - V(\mathrm{fcc\ Fe})] / V_H. \qquad (1)$$

Here we adopted the equation of state (EOS) of fcc Fe at 298 K (Boehler 1990). Note that spin transition in fcc Fe has not been observed in previous experiments (Tsujino et al. 2013), but is expected to occur within the studied pressure range. Volume expansion per H atom, V_H, is calculated for each pressure by the Vinet equation of state using K_0 =

99.2 GPa and $K'_0 = 3.98$ from Fukai (1992). For V_{H0}, we employed the value of 2.22 Å^3 based on neutron diffraction measurements of FeH_X up to 12 GPa and 1200 K (Ikuta et al. 2019), assuming that the pressure and temperature terms are compensated and the volume is close to that at 0 GPa and 300 K.

Our *ab initio* calculations produced lattice volumes of ferromagnetic (FM), antiferromagnetic (AFM), and nonmagnetic (NM) fcc FeH at high pressures. We used the Perdew-Burke-Ernzerhof (PBE) form (Perdew et al. 1996) of generalized-gradient approximation (GGA) for the exchange-correlation functional. Vanderbilt's type pseudopotentials were used (Vanderbilt 1990). The fcc unit cell contained 1 FeH. The cutoff radii for Fe and H were 0.956 and 0.265 Å, respectively. The plane-wave basis set with a cutoff energy of 40 Ry was used. The **k**-point mesh was 12×12×12. A smearing technique (Methfessel and Paxton 1989) was used for integration up to the Fermi surface with a smearing parameter of 0.01 Ry. We used the quasi-harmonic approximation to take phonon effects into account (Wallace 1972). Dynamical matrices were computed at the 4×4×4 **q**-point mesh using the density-functional-perturbation theory (Baroni et al. 2001; Giannozzi et al. 1991). Vibrational densities of states were obtained by interpolation of phonon frequencies on the 24×24×24 **q**-point mesh. We evaluated FM, AFM, and NM states. For AFM FeH, we considered two spin configurations: one designed to mimic AFM FeO with iron atoms on the (111) plane in the same spin and opposite spins on adjacent planes (Fig. S2a), and a second configuration with iron atoms on the (100) plane in the same spin state and opposite spins on adjacent planes (Fig. S2b). As the AFM spin configuration that mimics FeO has lower enthalpy in the pressure interval in which it was evaluated (-5 to 20 GPa), it is assumed to be more stable and is the only AFM structure discussed further in this text. All calculations were performed using the Quantum-ESPRESSO package (Giannozzi et al. 2009).

RESULTS AND DISCUSSION

We performed eight separate XRD experiments to examine the stable phase of FeH to 137 GPa (Fig. 1 and Table S2). At each *P-T* condition, we evaluated the stable phase of FeH_X from appearance/disappearance and growth/weakening of XRD peaks by increasing temperature with the fiber lasers. The hydrogen content (X) of each of the synthesized fcc FeH_X samples after laser heating was almost unity (Fig. 2a).

In runs #1–3, the iron sample and paraffin reacted to form iron carbide soon after the beginning of laser heating at around 1600 K and 60 GPa. After ~1-hour heating, iron carbide disappeared, and fcc FeH_X and diamond formed as previously reported (Narygina et al. 2011; Ohta et al. 2019; Thompson et al. 2018).

In the other five runs, we loaded H_2 cryogenically into the sample chamber with iron foil and then observed the chemical reaction between iron and H_2 at high pressures and temperatures. The occurrence of hydrogenation of the iron sample during the cryogenic H_2 loading depends on the *P*-*T* pathway. After H_2 was cryogenically loaded, but prior to heating, XRD from pure iron and the Raman peak of the H_2 vibration mode could be confirmed in 2 of the 5 samples prepared using this method, while in the other runs, we observed hcp or dhcp FeH_X after recovery from the helium refrigerator (Table S2). To facilitate the reaction, we annealed the sample at around 1000 K by laser heating. In four runs, FeH_2 or FeH_3 were observed occasionally, but weakened during continuous heating (Table S2).

In runs #4 and #5, the samples were determined to be at 126 and 106 GPa, respectively, when measured at room temperature subsequent to cryogenic H_2 loading. We observed XRD peaks from pure hcp Fe and Raman peak from H_2 vibration mode before heating. During laser heating, hcp Fe diffraction peaks weakened, and a diffused XRD signal appeared, and further heating ended up with the sudden emergence of XRD peaks from fcc FeH_X (Figs. 1a and S3). In run #5, after formation of fcc FeH_X, the sample was further compressed and pressure-volume data was obtained. At 137 GPa, the sample was heated again at around 1000 K. Growth of the peaks of fcc FeH_X was observed during heating, and we therefore interpreted this as meaning that fcc FeH_X is in a stable phase at this pressure and temperature.

In runs #6 and #7, hcp and dhcp FeH_X was already confirmed before heating at 85 and 70 GPa, respectively. The XRD peaks from dhcp FeH_X were replaced by those from fcc FeH_X during heating, indicating the dhcp to fcc transition (Fig. 1b). In run #6, after formation of fcc FeH_X, the sample was compressed and heated at 99 and 105 GPa, and then decompressed and heated at 72, 66, 55 and 25 GPa. As with run #5, the growth of peaks indicates that fcc FeH_X is stable at each pressure except 25 GPa. When the sample was heated at 25 GPa, the fcc peaks were drastically weakened and new peaks, possibly from dhcp FeH_X ($X<1$), appeared. Therefore, fcc FeH_X should no longer be stable at 25 GPa. The mean value of X for fcc FeH_X in runs #1~7 was 1.01(6) (Fig. 2a).

In run #8, we first observed dhcp FeH_X just after H_2 loading. The consequent reaction by laser annealing at 53 GPa was dhcp to hcp transition (Fig. S4). Hydrogen content in the hcp FeH_X sample was about 0.3, which indicates hcp phase is stable when hydrogen content is less than ~0.3 as reported by the literature (Antonov et al. 1998; Gomi et al. 2018; Machida et al. 2019; Yuan et al. 2018).

Based on the present and previous results, we confirmed that fcc FeH has a wider stability field than previously thought (Fig. 3). This suggests that prior studies observed metastable dhcp phase to 136 GPa because of an absence of thermal annealing (Badding et al. 1991; Hirao et al. 2004; Pépin et al. 2014; Shibazaki et al. 2012). A large energetic barrier for dhcp-fcc transition in FeH would exist. One can consider that there is no triple point of dhcp, fcc and liquid FeH, and that the dhcp phase has a closed stability region similar to the hcp phase of cobalt (Yoo et al. 2000) (Fig. 3). While previous theoretical studies have predicted the stability of hcp FeH at 300 K between about 40 and 80 GPa (Isaev et al. 2007), hcp FeH_X with X~1 was not stable in this study.

The volumes of synthesized nearly stoichiometric fcc FeH_X were collected with changing pressure, which is plotted in Figure 2b and summarized in Table S3. Our experimental *P-V* data exhibits a discontinuous change in compressibility at ~60 GPa. Note that the change in X at similar pressure can be attributed to this change in compressibility and is not truly compositional. We fitted the third-order Birch-Murnaghan EOS to the *P-V* data separately for the 15-57 GPa and 72-137 GPa pressure intervals (Table 1). The bulk modulus K_0 and its pressure derivative K_0' of the high-*P* EOS were larger and smaller than those of the low-*P* EOS, respectively.

The observed anomaly in compression behavior without structural change is possibly due to magnetic transition in fcc FeH. Thus, we calculated the volume of fcc FeH at high *P* considering its magnetism. In the static *ab initio* calculations for stoichiometric FeH, we obtained the FM state up to ~50 GPa, which is always stable with respect to the NM state. The AFM state is energetically never stable with respect to both the FM and NM states at all pressures investigated. Under compression, the magnetic moment (*M*) calculated for the FM state decreased gradually from 2.2 μ_B/FeH at 13.5 $Å^3$/FeH (i.e., 0 GPa) to 1.8 μ_B/FeH at ~11 $Å^3$/FeH corresponding to ~50 GPa

(Fig. 4). By further compression, however, M in the FM state abruptly vanished and the system became NM with an abrupt decrease in volume, a result qualitatively consistent with Isaev et al. (2007) and Elsässer et al. (1998). For comparison, we also calculated M in the dhcp and hcp phases under compression as shown in Figure 4. At low pressures (i.e., $V > 11$ Å^3/FeH), M in all three phases are similar to each other; that in fcc is marginally higher than those in the other two phases. In the dhcp phase, the magnetization abruptly vanished at ~10.3 Å^3/FeH, slightly smaller than that in fcc. In the hcp phase, on the other hand, magnetization behavior is rather different: the FM state survives down to ~8.5 Å^3/FeH (~210 GPa) with a continuous decrease in M. These magnetization behaviors are generally consistent with previous calculations (Isaev et al. 2007; Tsumuraya et al. 2012).

Calculated parameters of static and 300 K third-order Birch-Murnaghan EOS of the fcc phase are summarized in Table 1. As usual, the calculated 300 K volume is larger than the static one, which is mainly due to the effect of zero-point motion. The static FM and NM EOS are approximately consistent with earlier calculations (Bazhanova et al. 2012; Isaev et al. 2007). The values of V_0 and K_0 in the FM state are larger and smaller than those of NM, respectively. The 300 K *P-V* curve of FM and NM states are shown in Figure 2b. Comparison of the present experimental and computational *P-V* curves suggest that the change in compressibility can be attributed to a change in the elastic properties due to the FM-NM transition predicted by *ab initio* calculations. Another possibility is the change of site occupancy of H for the octahedral and tetrahedral interstitial sites in FeH_X. However, such an argument is beyond the scope of the present study because the site occupancy cannot be determined from XRD.

From the present experimental and computational results, the FM-NM transition pressure in fcc FeH is 50-60 GPa. On the other hand, Narygina et al. (2011) argued that fcc FeH was in the NM or AFM state at 26-47 GPa based on Mössbauer spectroscopy measurements. We point out that their Mössbauer spectra may not have captured the signal of fcc FeH alone, but was affected by the surrounding hcp Fe – which was not heated and hydrogenated – because the spot size of their Mossbauer spectrometer was ~10^3 times as large as the laser-heated spot, and ~10^4 times as large as the size of the X-ray beam used in their XRD experiments. Recently, Thompson et al. (2018) performed synchrotron Mössbauer spectroscopy on fcc FeH_X and found that spin transition is unlikely to occur at 64-82 GPa, suggesting fcc FeH_X is not ferromagnetic at these pressures.

IMPLICATIONS

In this study, we demonstrated that near-stoichiometric fcc FeH (rather than dhcp structure) with a nonmagnetic state was stable above ~70 GPa to 137 GPa (Fig. 3). Experimental and theoretical studies of FeH_X suggested that it is able to satisfy the density and sound velocity of the Earth's core, and is hence a strong candidate for a light element in the core (Hirose et al. 2019; Sakamaki et al. 2016; Tagawa et al. 2016; Umemoto and Hirose 2015). A precise *P*-*T*-*X* phase diagram of Fe-H at core pressures is key to constraining the temperature of the core and density contrast at the inner core-outer core boundary, but it has not been determined well because of the experimental difficulties even at very low pressure (e.g., Shibazaki et al. 2014). Fukai (1992) speculated a *P*-*T*-*X* phase diagram of the Fe–H alloy at about 100 GPa on the basis of the well-known phase diagrams of metal-hydrogen systems and thermodynamic functions. Fukai (1992) assumed that there was a continuous, subsolidus solid solution between hcp Fe and dhcp FeH at ~100 GPa. Our results rule out dhcp FeH as an endmember phase in the diagram because of the weakening of its XRD peaks in our laser heating experiments (Fig. 1b). Our finding suggests that the subsolidus phases in the Fe‑FeH system at about 100 GPa change with hydrogen content. At least three subsolidus phases would exit in the Fe-FeH binary region at the core conditions, since hcp FeH_X ($0.13<X<0.32$) and dhcp FeH_X ($0.41<X<0.90$) were observed up to 113 GPa and 2060 K as consequences of decomposition of hydrous mineral, and Fe and water reaction (Nishi et al. 2017; Yuan et al., 2018) in addition to the present study. Melting experiments on FeH_X by means of LHDAC demonstrated that $FeH_{1.02}$ melted at 108 GPa and 2260 K, and a more hydrogen-rich Fe melt ($FeH_{2.33}$) was made at 127 GPa and *T* less than 2120 K (Hirose et al. 2019) (Fig. 3). Some Fe polyhydrides could be stable as subsolidus phases in a Fe‑H system at Mbar pressure range (Bazhanova et al. 2012; Kvashnin et al. 2018; Pépin et al. 2014, 2017). The melting *T* of hydrogen at 100 GPa was determined to be 800~1000 K (Caillabet et al. 2011; Zha et al. 2017), while it was assumed to be 2500 K in Fukai (1992). Therefore, the *P-T-X* phase diagram of the Fe-H system at the core pressures range should be more complicated than we have ever thought. Subsolidus phases of FeH_X with various hydrogen contents and their melting temperatures at the core conditions are required to determine this in the future.

ACKNOWLEDGMENTS

We thank two anonymous reviewers for their constructive comments which improved the quality of the manuscript. *In-situ* XRD measurements were performed at BL10XU, SPring-8 (proposal no. 2014A0080, 2014B0080, 2015A0080, 2015B0080, and 2016B0080). Calculations were performed at ELSI and supported by JSPS Kakenhi (Grant number: 17K05627).

REFERENCES CITED

Antonov, V., Cornell, K., Fedotov, V., Kolesnikov, A., Ponyatovsky, E., Shiryaev, V., and Wipf, H. (1998) Neutron diffraction investigation of the dhcp and hcp iron hydrides and deuterides. Journal of Alloys and Compounds, 264, 214–222.

Badding, J.V., Hemley, R.J., and Mao, H.K. (1991) High-pressure chemistry of hydrogen in metals: in situ study of iron hydride. Science, 253, 421–424.

Baroni, S, Gironcoli, D.S., and of Physics, D.A. (2001) Phonons and related crystal properties from density-functional perturbation theory. Reviews of Modern Physics, 73, 516–558.

Bazhanova, Z., Oganov, A., and Gianola, O. (2012) Fe–C and Fe–H systems at pressures of the Earth's inner core. Physics-Uspekhi, 55, 489–497.

Boehler, R., von Bargen, N., and Chopelas, A. (1990) Melting, thermal expansion, and phase transitions of iron at high pressures. Journal of Geophysical Research, 95, 21731–21736.

Caillabet, L., Mazevet, S., and Loubeyre, P. (2011) Multiphase equation of state of hydrogen from *ab initio* calculations in the range 0.2 to 5 g/cc up to 10 eV. Physical Review B, 83, 094101.

Chi, Z., Nguyen, H., Matsuoka, T., Kagayama, T., Hirao, N., Ohishi, Y., and Shimizu, K. (2011) Cryogenic implementation of charging diamond anvil cells with H_2 and D_2. The Review of scientific instruments, 82, 105109.

Dewaele, A., Belonoshko, A., Garbarino, G., Occelli, F., Bouvier, P., Hanfland, M., and Mezouar, M. (2012) High-pressure–high-temperature equation of state of KCl and KBr. Physical Review B, 85, 214105.

Dorogokupets, P.I., and Oganov, A.R. (2007) Ruby, metals, and MgO as alternative pressure scales: A semiempirical description of shock-wave, ultrasonic, X-ray, and thermochemical data at high temperatures. Physical Review B, 75, 024115.

Elsässer, C., Zhu, J., Louie, S.G., and Meyer, B. (1998) *Ab initio* study of iron and iron hydride: II. Structural and magnetic properties of close-packed Fe and FeH. Journal of Physics: Condensed Matter, 10, 5113–5129.

Fukai, Y. (1992) Some properties of the Fe-H system at high pressures and temperatures, and their implications for the Earth's core. In Y . Syono and M.H. Manghnani, Eds., High Pressure Research: Application to Earth and Planetary Sciences, p. 373–385. TERRAPUB, Washington, D.C.

Giannozzi, P., Gironcoli, S., Pavone, P., and Baroni, S. (1990) *Ab initio* calculation of phonon dispersions in semiconductors. Physical Review B, 43, 7231–7242.

Giannozzi, P., Baroni, S., Bonini, N., Calandra, M., Car, R., Cavazzoni, C., Ceresoli, D., Chiarotti, G., Cococcioni, M., Dabo, I., and others (2009) QUANTUM ESPRESSO: a modular and open-source software project for quantum simulations of materials. Journal of Physics: Condensed Matter, 21, 395502.

Gomi, H., Fei, Y., and Yoshino, T. (2018) The effects of ferromagnetism and interstitial hydrogen on the equation of states of hcp and dhcp FeH_X: Implications for the Earth's inner core age. American Mineralogist, 103, 1271–1281.

Hirao, N., Kondo, T., Ohtani, E., Takemura, K., and Kikegawa, T. (2004) Compression of iron hydride to 80 GPa and hydrogen in the Earth's inner core. Geophysical Research Letters, 31, L06616.

Hirose, K., Tagawa, S., Kuwayama, Y., Sinmyo, R., Morard, G., Ohishi, Y., and Genda, Y. (2019) Hydrogen limits carbon in liquid iron. Geophysical Research Letters, 46, https://doi.org/10.1029/2019GL082591.

Ikuta, D., Ohtani, E., Sano-Furukawa, A., Shibazaki, Y., Terasaki, H., Yuan, L., and Hattori, T. (2019) Interstitial hydrogen atoms in face-centered cubic iron in the Earth's core. Scientific Reports, 9, 7108.

Isaev, E., Skorodumova, N., Ahuja, R., Vekilov, Y., and Johansson, B. (2007) Dynamical stability of Fe-H in the Earth's mantle and core regions. Proceedings of the National Academy of Sciences, 104, 9168–9171.

Kvashnin, A., Kruglov, I., Semenok, D., and Oganov, A. (2018) Iron superhydrides FeH_5 and FeH_6: Stability, electronic properties and superconductivity. The Journal of Physical Chemistry C, 122, 4731–4736.

Machida, A., Saitoh, H., Hattori, T., Sano-Furukawa, A., Funakoshi, K., Sato, T., Orimo, S., and Aoki, K. (2019) Hexagonal close-packed iron hydride behind the conventional phase diagram. Scientific Reports, 9, 12290.

Methfessel, M., and Paxton, A. (1989) High-precision sampling for Brillouin-zone integration in metals. Physical Review B, 40, 3616–3621.

Narygina, O., Dubrovinsky, L., McCammon, C., Kurnosov, A., Kantor, I., Prakapenka, V., and Dubrovinskaia, N. (2011) X-ray diffraction and Mössbauer spectroscopy study of fcc iron hydride FeH at high pressures and implications for the composition of the Earth's core. Earth and Planetary Science Letters, 307, 409–414.

Nishi, M., Kuwayama, Y., Tsuchiya, J., and Tsuchiya, T. (2017) The pyrite-type high-pressure form of FeOOH. Nature, 547, 205–208.

Ohishi, Y., Hirao, N., Sata, N., Hirose, K., and Takata, M. (2008) Highly intense monochromatic X-ray diffraction facility for high-pressure research at SPring-8. High Pressure Research, 28, 163–173.

Ohta, K., Ichimaru, K., Einaga, M., Kawaguchi, S., Shimizu, K., Matsuoka, T., Hirao, N., and Ohishi, Y. (2015) Phase boundary of hot dense fluid hydrogen. Scientific Reports, 5, 16560.

Ohta, K., Suehiro, S., Hirose, K., and Ohishi, Y. (2019) Electrical resistivity of fcc phase iron hydrides at high pressures and temperatures. Comptes Rendus Geoscience, 351, 147–153.

Pépin, C., Dewaele, A., Geneste, G., Loubeyre, P., and Mezouar, M. (2014) New iron hydrides under high pressure. Physical Review Letters, 113, 265504.

Pépin, C.M., Geneste, G., Dewaele, A., and Mezouar, M. (2017) Synthesis of FeH_5: A layered structure with atomic hydrogen slabs. Science, 357, 382–385.

Perdew, J., Burke, K., and Ernzerhof, M. (1996) Generalized gradient approximation made simple. Physical Review Letters, 78, 1396–1396.

Poirier, JP (1994) Light elements in the Earth's outer core: a critical review. Physics of the earth and planetary interiors, 85, 319–337.

Saitoh, H., Machida, A., Sugimoto, H., Yagi, T., and Aoki, K. (2017) *P–V–T* relation of the Fe–H system under hydrogen pressure of several gigapascals. Journal of Alloys and Compounds, 706, 520–525.

Sakamaki, K., Takahashi, E., Nakajima, Y., Nishihara, Y., Funakoshi, K., Suzuki, T., and Fukai Y. (2009) Melting phase relation of FeH_X up to 20 GPa: Implication for the temperature of the Earth's core. Physics of the Earth and Planetary Interiors, 174, 192–201.

Sakamaki, T., Ohtani, E., Fukui, H., Kamada, S., Takahashi, S., Sakairi, T., Takahata, A., Sakai, T., Tsutsui, S., Ishikawa, D., and others (2016) Constraints on Earth's inner core composition inferred from measurements of the sound velocity of hcp-iron in extreme conditions. Science Advances, 2, e1500802.

Seto, Y., Nishio-Hamane, D., Nagai, T., and Sata, N. (2010) Development of a software suite on X-ray diffraction experiments. The Review of High Pressure Science and Technology, 20, 269–276.

Shibazaki, Y., Ohtani, E., Fukui, H., Sakai, T., Kamada, S., Ishikawa, D., Tsutsui, S., Baron, A., Nishitani, N., Hirao, N., and others (2012) Sound velocity measurements in dhcp-FeH up to 70 GPa with inelastic X-ray scattering: Implications for the composition of the Earth's core. Earth and Planetary Science Letters, 313–314, 79–85.

Shibazaki, Y., Terasaki, H., Ohtani, E., Tateyama, R., Nishida, K., Funakoshi, K., and Higo, Y. (2014) High-pressure and high-temperature phase diagram for $Fe_{0.9}Ni_{0.1}$–H alloy. Physics of the Earth and Planetary Interiors, 228, 192–201.

Tagawa, S., Ohta, K., Hirose, K., Kato, C., and Ohishi, Y. (2016) Compression of Fe–Si–H alloys to core pressures. Geophysical Research Letters, 43, 3686–3692.

Thompson, E.C., Davis, A.H., Bi, W., Zhao, J., Alp, E.E., Zhang, D., Greenberg, E., Prakapenka, V.B., and Campbell A.J. (2018) High - pressure geophysical properties of fcc phase FeH_X. Geochemistry, Geophysics, Geosystems, 19, 305–314.

Tsujino, N., Nishihara, Y., Nakajima, Y., Takahashi, E., Funakoshi, K., and Higo, Y. (2013) Equation of state of γ-Fe: Reference density for planetary cores. Earth and Planetary Science Letters, 375, 244–253.

Tsumuraya, T., Matsuura, Y., Shishidou, T., and Oguchi, T. (2012) First-principles study on the structural and magnetic properties of iron hydride. Journal of the Physical Society of Japan, 81, 064707.

Ueda, Y., Matsui, M., Yokoyama, A., Tange, Y., and Funakoshi, K. (2008) Temperature-pressure-volume equation of state of the *B*2 phase of sodium chloride. Journal of Applied Physics, 103, 113513.

Umemoto, K., and Hirose, K. (2015) Liquid iron - hydrogen alloys at outer core conditions by first - principles calculations. Geophysical Research Letters, 42, 7513–7520.

Vanderbilt, D. (1990) Soft self-consistent pseudopotentials in a generalized eigenvalue formalism. Physical Review B, 41, 7892–7895.

Wallace, D.C. Thermodynamics of Crystals (Wiley, Hoboken, 1972).

Yoo, C., Cynn, H., Söderlind, P., and Iota, V. (2000) New β(fcc)-cobalt to 210 GPa. Physical Review Letters, 84, 4132–4135.

Yuan, L., Ohtani, E., Ikuta, D., Kamada, S., Tsuchiya, J., Naohisa, H., Ohishi, Y., and Suzuki, A. (2018) Chemical reactions between Fe and H_2O up to megabar pressures and implications for water storage in the Earth's mantle and core. Geophysical Research Letters, 45, 1330–1338.

Zha, C., Liu, H., Tse, J., and Hemley, R. (2017) Melting and high *P*-*T* transitions of hydrogen up to 300 GPa. Physical Review Letters, 119, 075302.

FIGURE CAPTIONS

FIGURE 1. Representative XRD patterns taken in runs #5 and #7. (**a**) Lower pattern, at 106 GPa before laser heating; middle, at 103 GPa after heating; upper, at 99 GPa after further heating. (**b**) Lower pattern, at 70 GPa before heating; upper, at 68 GPa after heating. Unknown peaks are marked as ?.

FIGURE 2. (a) Hydrogen content of FeH_X as a function of pressure calculated using Eq. (1). Closed and open symbols represent fcc and hcp FeH_X, respectively. Circles show FeH_X synthesized from iron and paraffin (runs #1–3) and squares show FeH_X synthesized from iron and H_2 (runs #4–8). **(b)** Volume per iron atom as a function of pressure for fcc FeH_X (X~1.0) and Fe. Symbols show experimental data for fcc FeH_X. Open circles, synthesized from iron and paraffin (runs #1–3, this study); open squares, from iron and H_2 (runs #4–7, this study); gray circles, from iron and paraffin (Narygina et al. 2011). Black lines correspond to the fit of the present experimental data with a third-order Birch-Murnaghan EOS for <60 GPa and >70 GPa. Light and dark gray lines

are the results of *ab initio* calculations for FM and NM fcc FeH. Dotted lines indicate extrapolation. Black dashed line represents the compression curve of iron (Boehler 1990).

FIGURE 3. Proposed pressure–temperature phase diagram of stoichiometric FeH_X ($X \sim 1$). Closed and open symbols indicate the stability of fcc and dhcp structures, respectively, from this study (circles) and earlier experimental results (squares, Sakamaki et al. (2009); diamond, Narygina et al. (2011); triangles, Thompson et al. (2018)). We recalculated the hydrogen content X for the data of Thompson et al. (2018) by using the method we employed, and plot them with $X \sim 1.0$. Asterisks indicate liquids (Sakamaki et al. 2009). Melting curve of FeH_X ($X \sim 1.0$) is from Hirose et al. (2019).

FIGURE 4. Magnetic moments calculated for fcc, dhcp, and hcp phases of stoichiometric FeH as a function of lattice volume. Dashed lines are guides for the eyes.

TABLE and FIGURES

TABLE 1. Parameters for fcc FeH third-order Birch-Murnaghan equation of states from experimental and ab initio calculations compared with previous

	V_0 (Å^3/Fe)	K_0 (GPa)	K_0'	Pressure range (GPa)	Temperature (K)	
experimental						
fcc FeH$_{x\sim1}$	13.8(7)	100(11)	9.3(16)	15-57	300	This study
	13.1(11)	227(8)	3.4(2)	72-137	300	This study
	13.5(1)	99(5)	11.7(5)	12-68	300	Narygina et al. (2011)
ab initio						
fcc FeH FM	13.5	168	4.5	<50 GPa	0	This study
	13.9	146	4.8	<50 GPa	300	This study
	13.9	155	3.7		0	Elsässer et al. (1998)
fcc FeH NM	12.3	262	4.2		0	This study
	12.6	242	4.3		300	This study
	12.2	271	4.3		0	Bazhanova et al. (2012)
	12.7	248	4.3		0	Elsässer et al. (1998)
Reference						
fcc Fe	11.3	165	5.5	0-16.8	300-1969	Boehler et al. (1990)

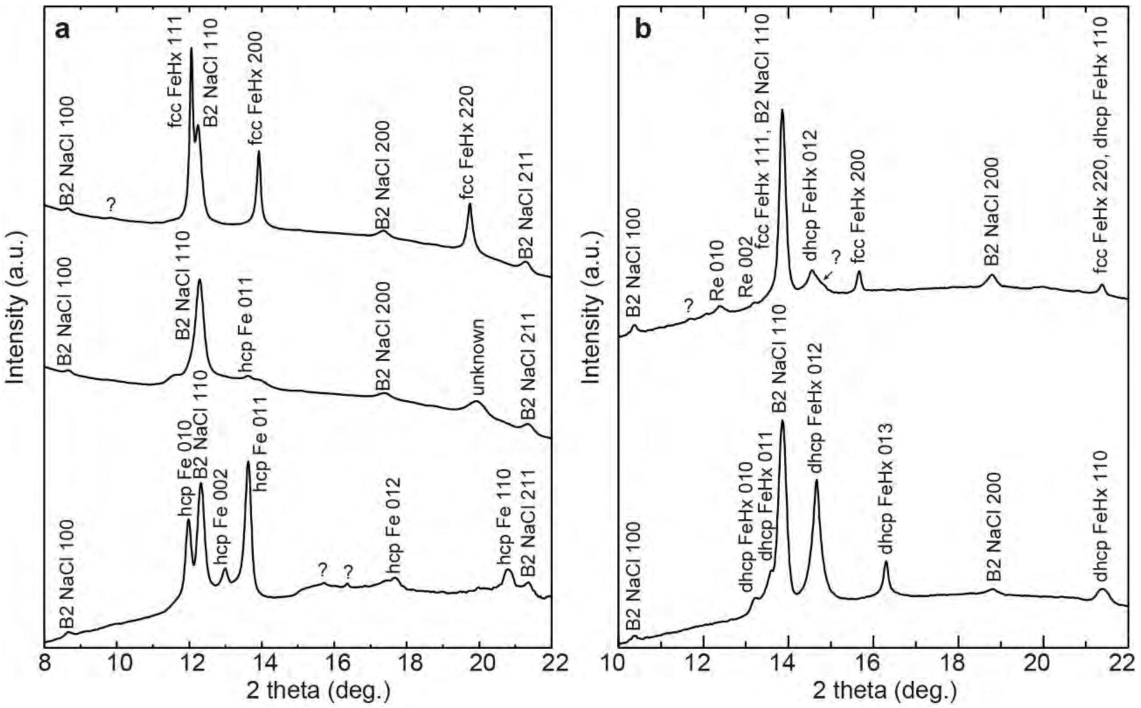
a
B2 NaCl 100
?
fcc FeHx 111
B2 NaCl 110
fcc FeHx 200
B2 NaCl 200
fcc FeHx 220
B2 NaCl 211
B2 NaCl 100
B2 NaCl 110
hcp Fe 011
B2 NaCl 200
unknown
B2 NaCl 211
B2 NaCl 100
hcp Fe 010
B2 NaCl 110
hcp Fe 002
hcp Fe 011
? ?
hcp Fe 012
hcp Fe 110
B2 NaCl 211
Intensity (a.u.)
2 theta (deg.)
8
10
12
14
16
18
20
22
b
B2 NaCl 100
?
Re 010
Re 002
fcc FeHx 111, B2 NaCl 110
dhcp FeHx 012
?
fcc FeHx 200
B2 NaCl 200
fcc FeHx 220, dhcp FeHx 110
B2 NaCl 100
dhcp FeHx 010
dhcp FeHx 011
B2 NaCl 110
dhcp FeHx 012
dhcp FeHx 013
B2 NaCl 200
dhcp FeHx 110
Intensity (a.u.)
2 theta (deg.)
10
12
14
16
18
20
22

FIGURE 1.

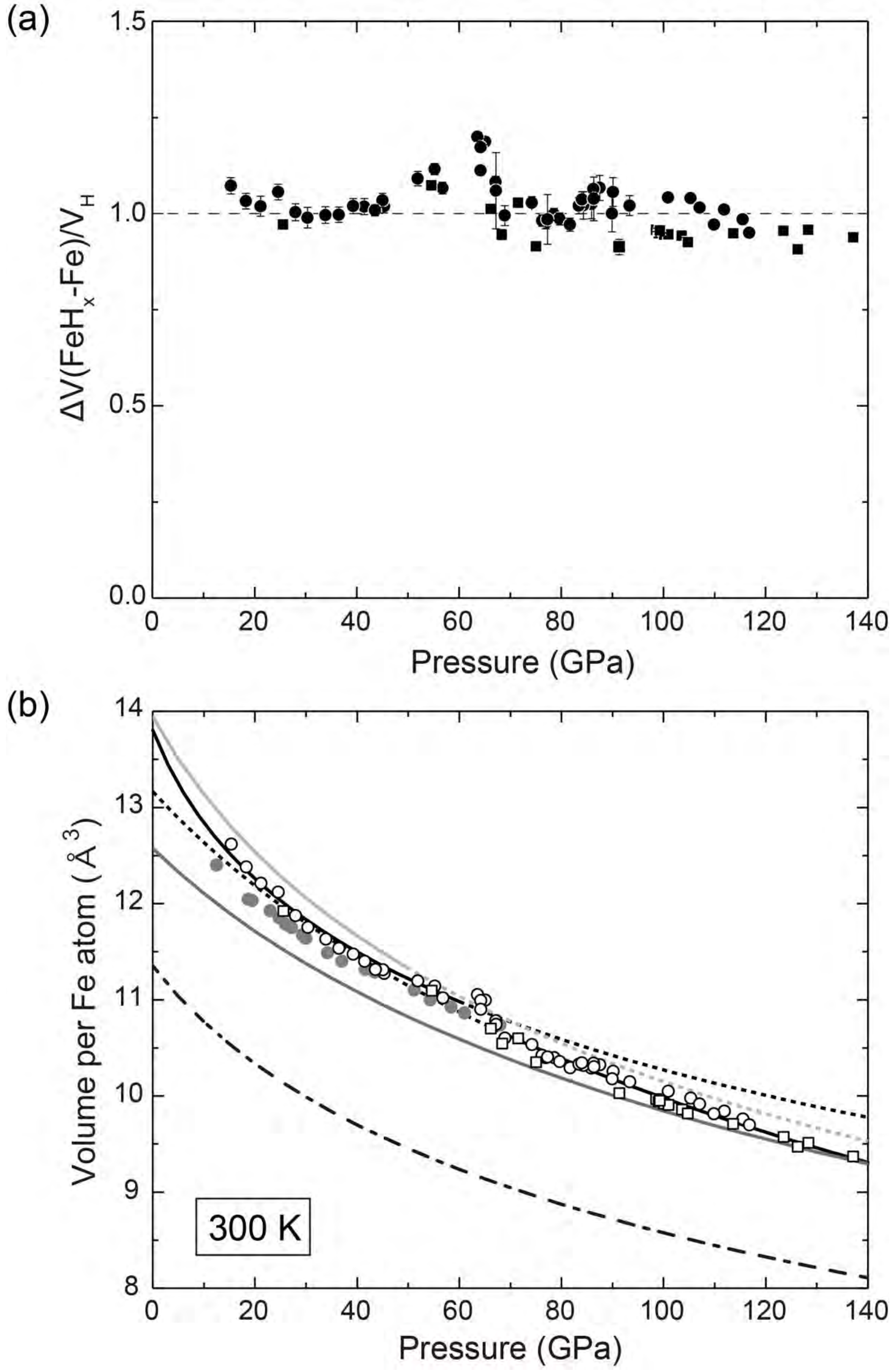

458

459 **FIGURE 2.**

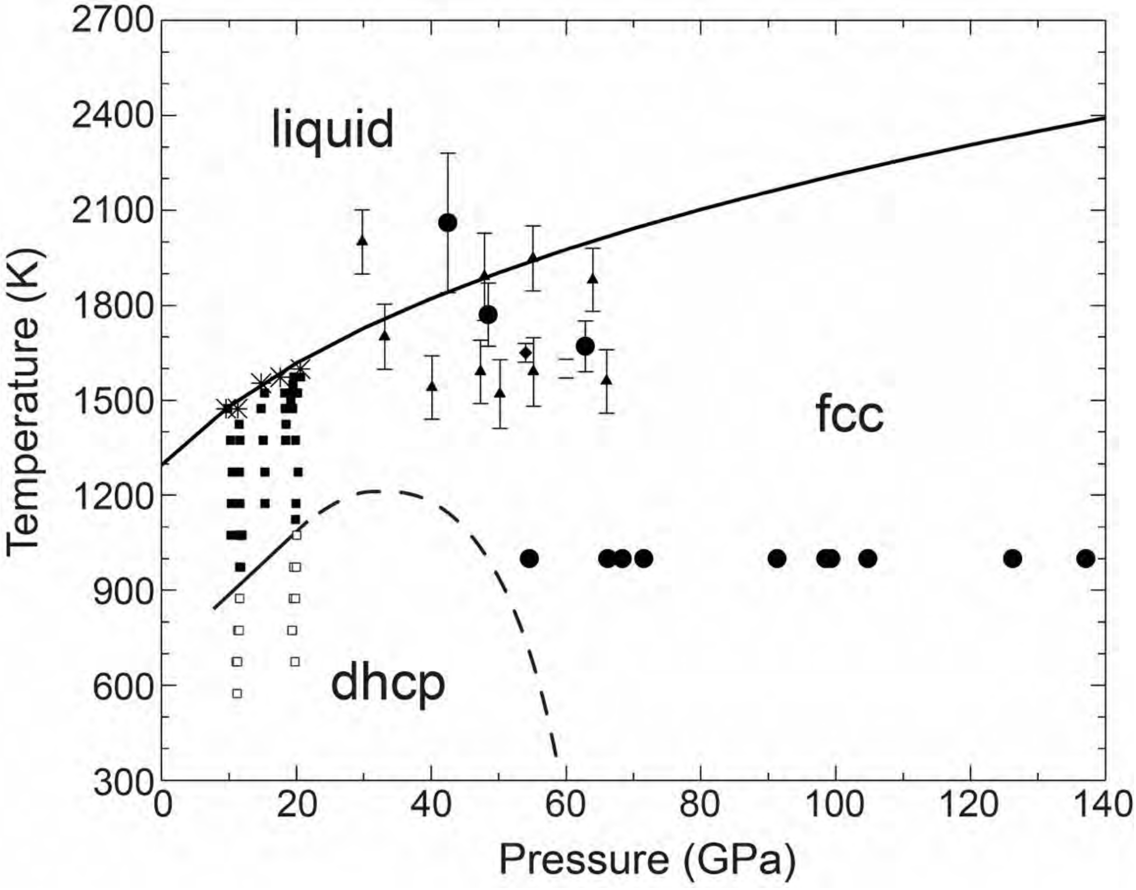

460

461 **FIGURE 3.**

462

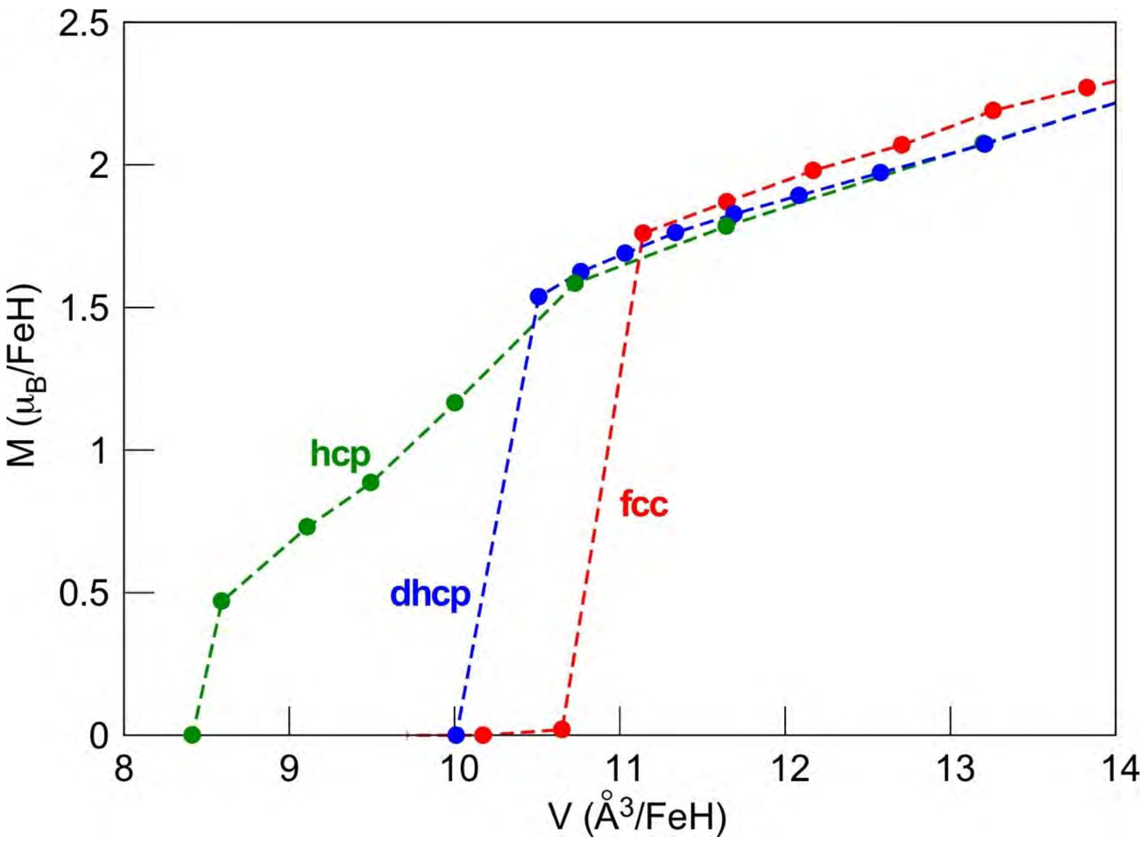

463

464 **FIGURE 4.**

TABLE 1. Parameters for fcc FeH third-order Birch-Murnaghan equation of states from expe

	V_0 (Å^3/Fe)	K_0 (GPa)	K_0'	Pressure range (GPa)
experimental				
fcc FeH$_{x\sim1}$	13.8(7)	100(11)	9.3(16)	15-57
	13.1(11)	227(8)	3.4(2)	72-137
	13.5(1)	99(5)	11.7(5)	12-68
ab initio				
fcc FeH FM	13.5	168	4.5	<50 GPa
	13.9	146	4.8	<50 GPa
	13.9	155	3.7	
fcc FeH NM	12.3	262	4.2	
	12.6	242	4.3	
	12.2	271	4.3	
	12.7	248	4.3	
Reference				
fcc Fe	11.3	165	5.5	0-16.8

rimental and ab initio calculations compared with previous studies.

Temperature (K)	
300	This study
300	This study
300	Narygina et al. (2011)
0	This study
300	This study
0	Elsässer et al. (1998)
0	This study
300	This study
0	Bazhanova et al. (2012)
0	Elsässer et al. (1998)
300-1969	Boehler et al. (1990)